hypofractionated radiation therapy. *Radiother Oncol* 2009;91: 307–313.
13. Semenenko VA, Li XA. Lyman-Kutcher-Burman NTCP model parameters for radiation pneumonitis and xerostomia based on combined analysis of published clinical data. *Phys Med Biol* 2008;53:737–755.
14. Yamashita H, Nakagawa K, Nakamura N, *et al.* Exceptionally high incidence of symptomatic grade 2-5 radiation pneumonitis after stereotactic radiation therapy for lung tumors. *Radiat Oncol* 2007;2:1–11.
15. Lebesque JV, Keus RB. The simultaneous boost technique: the concept of relative normalized total dose. *Radiother Oncol* 1991;22:45–55.
16. Lyman JT. Complication probability as assessed from dose-volume histograms. *Radiat Res Suppl* 1985;8:S13–S19.
17. Seppenwoolde Y, Lebesque JV, De Jaeger K, *et al.* Comparing different NTCP models that predict the incidence of radiation pneumonitis. Normal tissue complication probability. *Int J Radiat Oncol Biol Phys* 2003;55:724–735.
18. Venzon DJ, Moolgavkar SH. A method for computing profile-likelihood-based confidence intervals. *Applied Statistics* 1988; 37:87–94.
19. Clayton D, Hills M. Statistical models in epidemiology. Oxford University Press; New york: 1993.
20. Kwa SL, Theuws JC, Wagenaar A, *et al.* Evaluation of two dose-volume histogram reduction models for the prediction of radiation pneumonitis. *Radiother Oncol* 1998;48:61–69.
21. Claude L, Perol D, Ginestet C, *et al.* A prospective study on radiation pneumonitis following conformal radiation therapy in non-small-cell lung cancer: Clinical and dosimetric factors analysis. *Radiother Oncol* 2004;71:175–181.
22. Fujino M, Shirato H, Onishi H, *et al.* Characteristics of patients who developed radiation pneumonitis requiring steroid therapy after stereotactic irradiation for lung tumors. *Cancer J* 2006;12: 41–46.
23. Hernando ML, Marks LB, Bentel GC, *et al.* Radiation-induced pulmonary toxicity: a dose-volume histogram analysis in 201 patients with lung cancer. *Int J Radiat Oncol Biol Phys* 2001; 51:650–659.
24. Inoue A, Kunitoh H, Sekine I, *et al.* Radiation pneumonitis in lung cancer patients: A retrospective study of risk factors and the long-term prognosis. *Int J Radiat Oncol Biol Phys* 2001; 49:649–655.
25. Kim TH, Cho KH, Pyo HR, *et al.* Dose-volumetric parameters for predicting severe radiation pneumonitis after three-dimensional conformal radiation therapy for lung cancer. *Radiology* 2005;235:208–215.
26. Moreno M, Aristu J, Ramos LI, *et al.* Predictive factors for radiation-induced pulmonary toxicity after three-dimensional conformal chemoradiation in locally advanced non-small-cell lung cancer. *Clin Transl Oncol* 2007;9:596–602.
27. Oh D, Ahn YC, Park HC, *et al.* Prediction of radiation pneumonitis following high-dose thoracic radiation therapy by 3 Gy/fraction for non-small cell lung cancer: analysis of clinical and dosimetric factors. *Jpn J Clin Oncol* 2009;39:151–157.
28. Rancati T, Ceresoli GL, Gagliardi G, *et al.* Factors predicting radiation pneumonitis in lung cancer patients: A retrospective study. *Radiother Oncol* 2003;67:275–283.
29. Rodrigues G, Lock M, D'Souza D, *et al.* Prediction of radiation pneumonitis by dose-volume histogram parameters in lung cancer–A systematic review. *Radiother Oncol* 2004;71:127–138.
30. Schallenkamp JM, Miller RC, Brinkmann DH, *et al.* Incidence of radiation pneumonitis after thoracic irradiation: Dose-volume correlates. *Int J Radiat Oncol Biol Phys* 2007;67:410–416.
31. Tucker SL, Liu HH, Liao Z, *et al.* Analysis of radiation pneumonitis risk using a generalized Lyman model. *Int J Radiat Oncol Biol Phys* 2008;72:568–574.
32. Willner J, Jost A, Baier K, *et al.* A little to a lot or a lot to a little? An analysis of pneumonitis risk from dose-volume histogram parameters of the lung in patients with lung cancer treated with 3-D conformal radiotherapy. *Strahlenther Onkol* 2003; 179:548–556.
33. Kocak Z, Borst GR, Zeng J, *et al.* Prospective assessment of dosimetric/physiologic-based models for predicting radiation pneumonitis. *Int J Radiat Oncol Biol Phys* 2007;67:178–186.
34. van der Kogel AJ. Chronic effects of neutrons and charged particles on spinal cord, lung, and rectum. *Radiat Res Suppl* 1985;8:S208–S216.
35. Douglas BG, Fowler JF. The effect of multiple small doses of x rays on skin reactions in the mouse and a basic interpretation. *Radiat Res* 1976;66:401–426.
36. Curtis SB. Lethal and potentially lethal lesions induced by radiation--A unified repair model. *Radiat Res* 1986;106:252–270.
37. Joiner MC. Quantifying cell kill and cell survival. In: van der Kogel AJ, Joiner MC, editors. Basic clinical radiobiology, 4th ed. Hodder Arnold, London, UK; 2009. p. 42–55.
38. Fowler JF. The linear-quadratic formula and progress in fractionated radiotherapy. *Br J Radiol* 1989;62:679–694.
39. Kwa SL, Lebesque JV, Theuws JC, *et al.* Radiation pneumonitis as a function of mean lung dose: An analysis of pooled data of 540 patients. *Int J Radiat Oncol Biol Phys* 1998;42:1–9.
40. Thames HD, Bentzen SM, Turesson I, *et al.* Time-dose factors in radiotherapy: A review of the human data. *Radiother Oncol* 1990;19:219–235.
41. Van Dyk J, Mah K, Keane TJ. Radiation-induced lung damage: Dose-time-fractionation considerations. *Radiother Oncol* 1989; 14:55–69.
42. Bentzen SM, Joiner MC. The linear-quadratic approach in clinical practice. In: van der Kogel AJ, Joiner MC, editors. Basic clinical radiobiology. 4th ed. Hodder Arnold; 2009. p. 120–134.
43. Terry NH, Tucker SL, Travis EL. Residual radiation damage in murine lung assessed by pneumonitis. *Int J Radiat Oncol Biol Phys* 1988;14:929–938.
44. Okamoto Y, Murakami M, Yoden E, *et al.* Reirradiation for locally recurrent lung cancer previously treated with radiation therapy. *Int J Radiat Oncol Biol Phys* 2002;52:390–396.

ELSEVIER

Int. J. Radiation Oncology Biol. Phys., Vol. 77, No. 2, pp. 630–636, 2010

0360-3016/$–see front matter

doi:10.1016/j.ijrobp.2009.08.060

PHYSICS CONTRIBUTION

EVALUATION OF THE EFFECTIVENESS OF THE STEREOTACTIC BODY FRAME IN REDUCING RESPIRATORY INTRAFRACTIONAL ORGAN MOTION USING THE REAL-TIME TUMOR-TRACKING RADIOTHERAPY SYSTEM

GERARD BENGUA, PH.D.,* MASAYORI ISHIKAWA, PH.D.,* KENNETH SUTHERLAND,* KENJI HORITA, R.T.,† RIE YAMAZAKI, R.T.,† KATSUHISA FUJITA, R.T.,† RIKIYA ONIMARU, M.D.,‡ NORIWO KATOH, M.D.,‡ TETSUYA INOUE, M.D.,‡ SHUNSUKE ONODERA, M.D.,‡ AND HIROKI SHIRATO, M.D.‡

From the *Department of Medical Physics, †Radiology Department, and ‡Graduate School of Medicine, Hokkaido University, Sapporo, Hokkaido, Japan

Purpose: To evaluate the effectiveness of the stereotactic body frame (SBF), with or without a diaphragm press or a breathing cycle monitoring device (Abches), in controlling the range of lung tumor motion, by tracking the real-time position of fiducial markers.

Methods and Materials: The trajectories of gold markers in the lung were tracked with the real-time tumor-tracking radiotherapy system. The SBF was used for patient immobilization and the diaphragm press and Abches were used to actively control breathing and for self-controlled respiration, respectively. Tracking was performed in five setups, with and without immobilization and respiration control. The results were evaluated using the effective range, which was defined as the range that includes 95% of all the recorded marker positions in each setup.

Results: The SBF, with or without a diaphragm press or Abches, did not yield effective ranges of marker motion which were significantly different from setups that did not use these materials. The differences in the effective marker ranges in the upper lobes for all the patient setups were less than 1mm. Larger effective ranges were obtained for the markers in the middle or lower lobes.

Conclusion: The effectiveness of controlling respiratory-induced organ motion by using the SBF+diaphragm press or SBF + Abches patient setups were highly dependent on the individual patient reaction to the use of these materials and the location of the markers. They may be considered for lung tumors in the lower lobes, but are not necessary for tumors in the upper lobes. © 2010 Elsevier Inc.

Organ motion, Body frame, Real-time tracking, Effective range.

INTRODUCTION

The risk of radiation-induced lung complications may be minimized if intrafractional tumor motion caused by respiration during irradiation can be accurately accounted for. Various approaches to the management of respiratory motion in radiation therapy are comprehensively discussed in the American Association of Physicists in Medicine (AAPM) Report 91 (1). These include the accurate tracking of organ and tumor motion during treatment and methods by which the motion may be restricted or dampened.

Motion tracking may be accomplished by taking two sets of fluoroscopic images of the tumor itself, other anatomical structures, or fiducial markers placed near the tumor (2–4). Ideally, the function of real-time tracking is to determine the full range of tumor motion, as well as its trajectory during treatment from these fluoroscopic images taken at high frequency. At present, this is only possible in a few centers that have facilities dedicated for this purpose, such as the real-time tumor-tracking radiation therapy system developed at Hokkaido University Hospital (5, 6).

Restriction of respiration, on the other hand, can be achieved by using patient immobilization and by applying abdominal pressure. In extracranial stereotactic irradiation, Lax *et al.* (7), Herfarth *et al.* (8), and Negoro *et al.* (9) have reported the effectiveness of an abdominal press in reducing respiratory-induced tumor movement in stereotactic conformal radiation therapy of body tumors. Alternatively, an

Reprint requests to: Gerard Bengua, Department of Medical Physics, Hokkaido University Hospital, North-15 West-7, Kita-ku, Sapporo, 060-8648, Japan. Tel: (+81) 11-706-7638; Fax: (+81) 11-706-7639; E-mail: gerard@med.hokudai.ac.jp

The physics part of this study was supported by the grant-in-aid from the Japanese Ministry of Education, Culture, Sports, Science and Technology; the clinical portion was supported by the grant-in-aid from the Japanese Ministry of Health and Welfare.

Conflict of interest: This study was conducted in cooperation with Elekta Oncology Systems, Japan.

Acknowledgment—The authors express their gratitude to Drs. Shinichi Shimizu, Hiroshi Taguchi, and Mylin Torres for their help with the clinical aspects of this study.

Received Feb 18, 2009, and in revised form Aug 3, 2009. Accepted for publication Aug 19, 2009.

air-injected blanket has also been suggested for abdomen compression and fixation (10) to reduce breathing-induced organ motion.

In this study, we evaluated the effectiveness of a body frame and its combination with a diaphragm press in restricting the range of lung tumor motion by tracking the three-dimensional real-time position of fiducial gold markers embedded near the tumor. We also investigated the effect on respiratory-induced organ motion of using the stereotactic body frame (SBF) together with a breathing cycle monitoring device (Abches), which was used to self-regulate the patient's breathing cycle.

MATERIALS AND METHODS

The real-time tumor-tracking radiotherapy system

The three-dimensional trajectories of fiducial markers near or at tumor sites were tracked via the real-time tumor-tracking radiotherapy (RTRT) system at the Radiotherapy Department of Hokkaido University Hospital (5, 6, 11, 12). This fluoroscopy-based system is composed of two pairs of an X-ray source and image intensifier and an image acquisition and recognition unit that is interfaced with a linear accelerator to perform gated-irradiation. The positions of the gold markers were acquired every 0.033 s.

Body frame, diaphragm press, and breathing cycle monitor

For patient immobilization, we used Elekta's SBF (Elekta Oncology Systems) (13, 14). The same body frame was used in an earlier investigation on respiratory tumor movement and setup error verification using X-ray simulator images (7, 9, 15). The SBF is made from a rigid material formed into a half-hexagonal shell that wraps around the patient's torso. Because of the restricted space inside the shell, the patient's arms had to be positioned outside the shell by raising them above the head. Patient fixation inside the body frame was accomplished by means of a vacuum pillow, the size of which was chosen to ensure that it could provide an exact fit to the patient's body contour.

An additional accessory to the SBF was a frame that supports a pentagonal plastic plate that can be placed against the patient's abdomen to restrict the diaphragm motion. The pressure applied by the plate was regulated depending on the tolerance of each patient and was used only in the part of our measurements where its effectiveness to control motion from respiration was evaluated.

A breathing cycle monitor (commercially available as Abches [APEX Medical Inc., Tokyo, Japan]) was also used in combination with the body frame to investigate whether self-regulated breathing can reduce the amplitude of respiratory-induced tumor and organ motion. As shown in Fig. 1, the Abches consists of two extended arms, one for detecting abdominal movement and the other for detecting chest movement, and a respiration range indicator visible to the patient through a mirror attached to the head during the measurement.

Patient demographics

The patient population for this study was composed of 16 males and 3 females who were scheduled to undergo radiation therapy using the RTRT system in our hospital between 2006 and 2008. Table 1 shows the characteristics of the cohort for this study. The patients' ages ranged between 59 and 85 years (mean, 76 years). Fourteen patients had T1 lung cancer, whereas 5 had T2 and 1 had T3. No patient had lymph nodes irradiation and none of the patients had metastasis. Four patients had partial lung resection before the irradiation.

Table 1. Characteristics of the cohort for this study

Parameters	Number of patients
Sex	
Male	16
Female	3
Age range	59–85 (mean, 76)
Gold marker locations	
Upper right lobe	5
Middle lobe	1
Lower right lobe	4
Upper left lobe	6
Lower left lobe	3
Cancer classification	
T1N0M0	13
T2N0M0	5
T3N0M0	1

The locations of the gold markers were judged based on where they appeared in the computed tomography images of the patient. We classified the sample population into "upper lobe" or "middle or lower lobe" patients according to the location of gold markers in the lungs, because it has been reported that the relative locations in

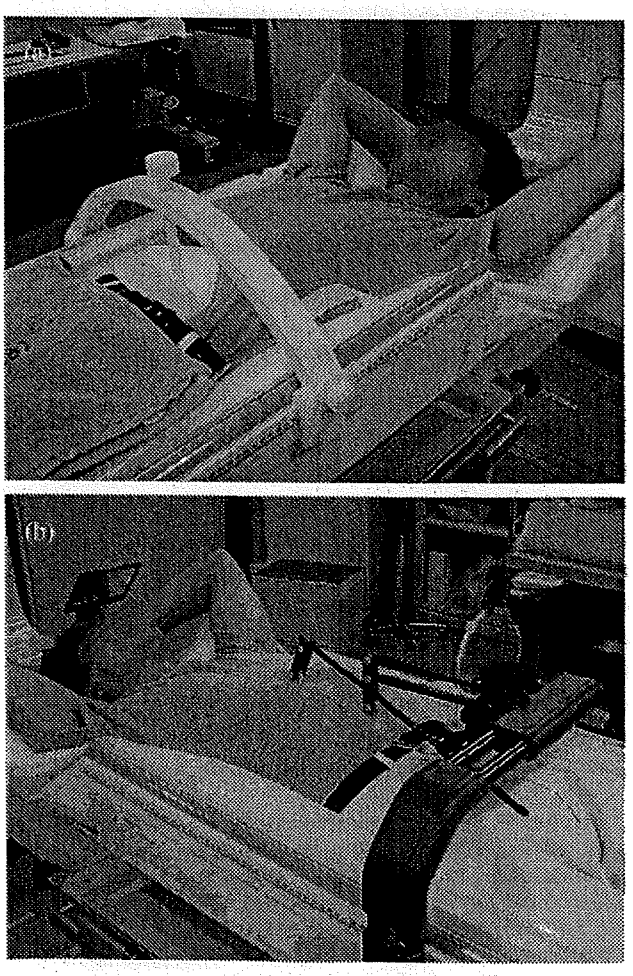

Fig. 1. Patient set-ups using the (a) stereotactic body frame (SBF)+diaphragm press (left) and the (b) SBF + Abches (right).

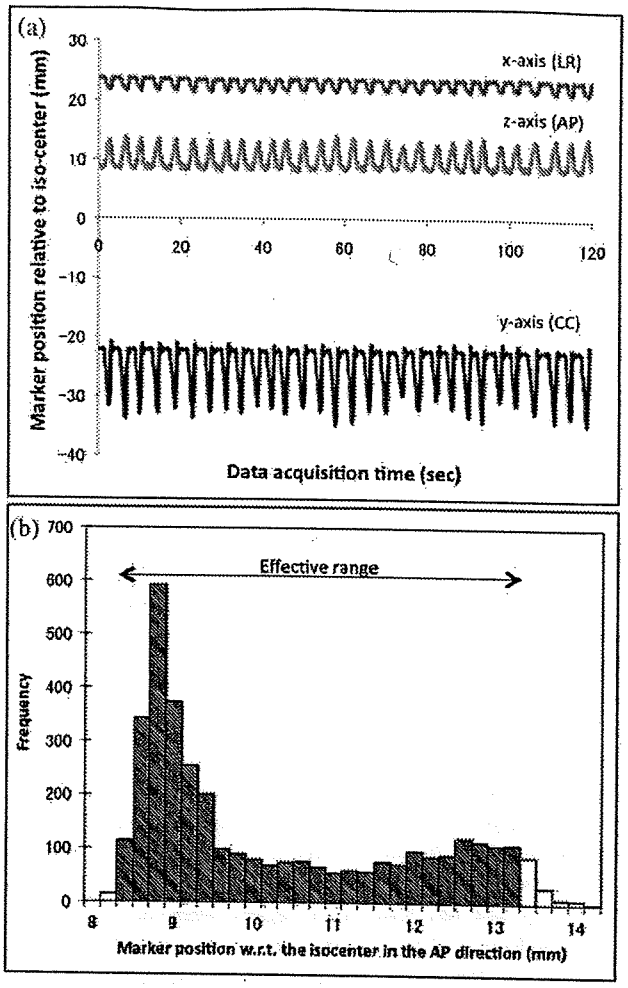

Fig. 2. Shown in (a) is an example of a 2-min tracking of the data from which the effective range was computed. The effective range along the z axis of the data in (a) is shown in (b).

the lung of the gold marker (16) and the tumor itself (17) influence the amplitude of their respective motions. Eleven of the 19 patients who participated in this study had gold markers embedded in the upper lobes of their lungs: 6 of the 11 had markers in the upper left and the other 5 had markers in the upper right. There was 1 patient with markers in the middle lobe and 7 patients with markers in either the lower left or lower right lobes of the lung.

Patient setup

Fluoroscopic tracking of the fiducial markers was performed in five different setups for each patient. In the first setup, the patient was made to lie on the treatment couch in the supine position with arms on the side. This was set as the reference patient position. In the second setup, the patient's arms were placed overhead to mimic the patient position when an SBF is used. The arms were not fixed into any structures, but were supported by cushions for patient comfort. The patient was asked to lie in the SBF in the third setup. Figure 1a shows the fourth setup, in which respiration was restricted using a plastic plate that pressed against the patient's diaphragm. In the fifth setup, shown in Fig. 1b, the Abches was attached to the SBF in the same manner as the abdominal press. The patients were able to monitor the relative amplitude of their breathing cycle from a respiration range indicator which was visible to the patient through a mirror.

Marker tracking

Tumor motion was monitored in real time by using 2-mm diameter gold markers, which were surgically placed near the tumor site and served as surrogate indicators of lung tumor motion (4). Three tracking measurements lasting for 5 min (2 min of tracking plus 3 min of rest) each were performed for every patient setup. The range of patient dose for the entire duration of marker tracking was between 14 and 591 mGy based on the estimates of Shirato *et al.* (18). Because the absorbed dose in the patient is strongly dependent on the tube voltage and pulse width, the X-ray tube settings were kept as low as possible during all the measurements.

Evaluation index and statistical analysis

The three-dimensional position of the gold marker relative to the iso-center is estimated by the RTRT system as it tracks the marker's motion. Sample tracking data are shown in Fig. 2a. The *effective range* of marker motion along each coordinate axis was computed about the mean marker position from the respective 2-min set of tracking data. Histograms similar to Fig. 2b with 0.2-mm position bins were constructed for each coordinate axis. The frequencies of the adjacent bins to the left and to the right of the median were accumulated until 95% of the total marker position frequency was achieved. The range of the included position bins was then defined as the *effective range* of the marker motion. The effective range along the z axis of the data in Fig. 2a is given as an example in Fig. 2b. A smaller effective range of the gold marker indicates less respiratory-induced organ motion.

The Mann-Whitney test was applied to assess the statistical significance of the differences in the effective ranges obtained between the reference setup and the other four setups.

This study was thoroughly discussed with the institutional review board of our hospital and its approval was received before the commencement of the measurements. Written patient consent was also received from all the participants in this research.

RESULTS

The effective ranges were observed to vary from patient to patient. In the reference setup (no SBF-arms down setup), the range was 0.60–5.27 mm, 0.93–19.93 mm, and 1.00–10.20 mm along the left-right (LR), craniocaudal (CC), and anteroposterior (AP) directions, respectively, among the 19 patients. The tumor motion, as indicated by the effective range of the tracked gold marker, was reduced in some patients by changing the patient setup, such as by placing the patient's arms overhead or by using the SBF and diaphragm press or Abches. However, this was not true for all the patients, because there were those whose range of tumor motion became worse in the setups other than the reference setup. Because of the small number of patients, we grouped the tumors into two categories: upper lobe and middle or lower lobe. In the reference setup, the CC direction yielded a significant difference in the mean effective range of the upper and middle or lower lobe markers, with a p value of 0.02. On the other hand, the differences in the mean effective range of markers in the upper lobe and the middle or lower lobes were not statistically significant for either the LR or AP direction in the reference setup.

We compared the effectiveness of each setup in reducing respiratory-induced intrafractional organ motion. Table 2

Table 2. Comparison between the mean effective ranges of motion (±1 SD) of the markers in the upper and middle or lower lobes for the 5 patient setups evaluated

		LR	CC	AP
No SBF, arms down (nSBF_AD)	Upper	2.15 ± 0.89 (0.60–3.20)	4.59 ± 3.01 (0.93–9.53)	3.39 ± 1.42 (1.00–5.87)
	Middle or lower	2.18 ± 1.60 (0.60–5.27)	10.93 ± 6.36 (1.07–19.93)	4.33 ± 3.05 (1.13–10.20)
	p value	0.66	0.02	0.72
No SBF, arms up (nSBF_AU)	Upper	2.21 ± 0.96 (0.67–3.73)	4.51 ± 3.06 (0.87–10.13)	3.23 ± 1.63 (1.00–6.27)
	Middle or lower	2.55 ± 1.56 (0.67–5.60)	10.6 ± 6.09 (1.07–19.00)	3.91 ± 2.45 (1.33–8.27)
	p value	0.72	0.03	0.72
With SBF (wSBF)	Upper	1.97 ± 0.89 (0.67–3.33)	4.23 ± 2.76 (0.67–9.53)	3.04 ± 1.54 (1.07–5.67)
	Middle or lower	2.98 ± 2.41 (0.87–6.93)	9.91 ± 5.67 (1.07–16.87)	4.43 ± 3.63 (0.93–10.60)
	p value	0.78	0.03	0.84
With SBF + diaphragm press (wSBF + DP)	Upper	1.95 ± 0.86 (0.60–3.33)	3.77 ± 2.57 (0.80–8.60)	3.09 ± 1.33 (1.20–5.27)
	Middle or lower	2.53 ± 2.23 (0.73–7.60)	9.43 ± 5.56 (0.80–16.33)	3.61 ± 2.64 (0.67–8.93)
	p value	0.90	0.03	0.97
With SBF + Abches (wSBF + Ac)	Upper	1.91 ± 0.81 (0.60–2.93)	3.98 ± 2.68 (0.73–8.33)	2.88 ± 1.23 (1.20–4.60)
	Middle or lower	3.27 ± 2.70 (0.67–7.73)	12.84 ± 6.37 (1.00–18.87)	5.04 ± 4.81 (0.93–13.40)
	p value	0.89	0.01	0.60

Abbreviations: LR = left-right; AP = anteroposterior; CC = craniocaudal; SBF = stereotactic body frame.
Given in brackets are the minimum and maximum effective ranges. The *p* values listed here are derived from the Mann-Whitney test.

shows the mean effective ranges of marker motion for all the patients in the five setups evaluated in this study. Also listed in Table 2 are the *p* values obtained from the nonparametric comparison of the mean effective marker range between the upper and the middle or lower groups of patients for each setup using the Mann-Whitney test. Measurements using these setups were carried out for all the patients except for 2 patients who decided not to continue with the measurements after the fourth setup. The sequences of setups for the tracking sessions were randomly changed between patients to minimize the possible bias from the setup sequence. Results of the RTRT measurement of the effective range of motion of fiducial markers showed that the use of the SBF, diaphragm press, or breathing cycle monitor to control the patient's breathing did not generally yield smaller effective marker ranges either for tumors in the upper lobe or those in the middle or lower lobes.

Motion of markers in the upper lobe

The mean effective ranges in the LR direction of the markers in the upper lobe showed little variation among the different patient setups. In the LR direction, they were around 2 mm for all setups (Fig. 3). The differences between the reference setup and the four other setups were no more than 1 mm, and none of these differences were statistically significant at the 5% level. Along the CC direction, the average effective ranges of the markers in the 5 setups were between 3.77 mm and 4.59 mm (Fig. 4). The mean and median of the effective range were around 2.88 mm to

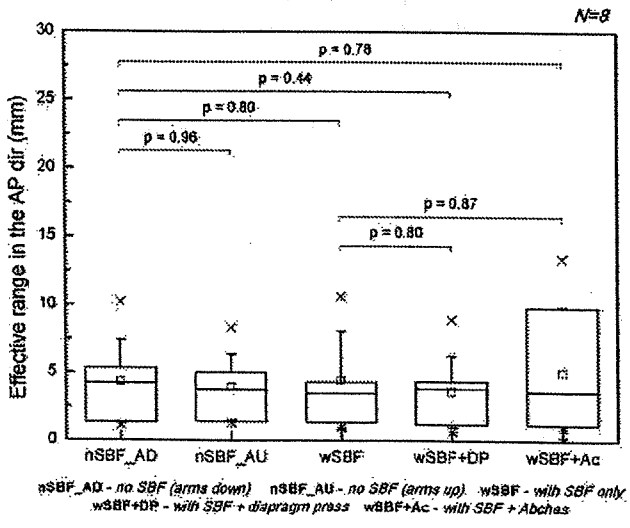

Fig. 3. The effective range along the lateral direction of the gold markers in the upper lobes of the lung. Also indicated are the *p* values obtained from comparison of the effective ranges obtained in each patient setup.

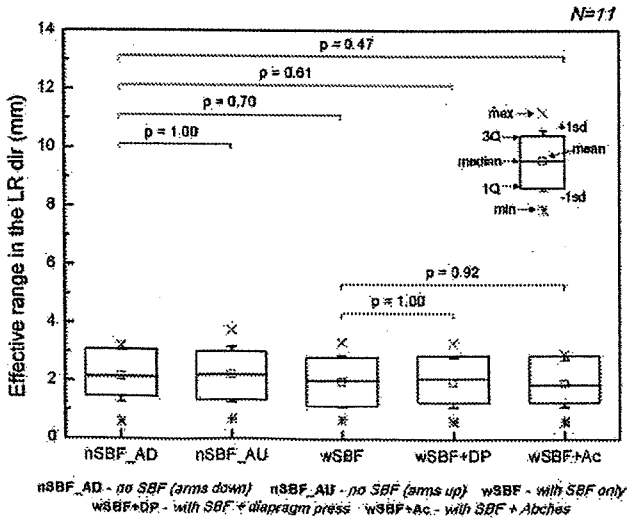

Fig. 4. The effective range along the craniocaudal direction of the gold markers in the upper lobes of the lung. Also indicated are the *p* values obtained from comparison of the effective ranges obtained in each patient setup.

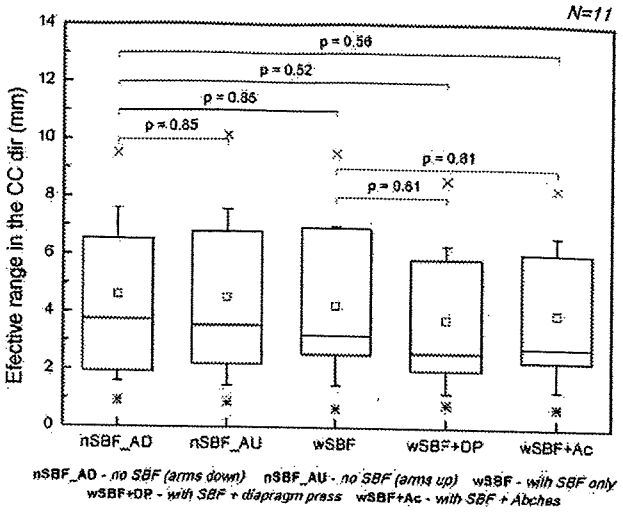

Fig. 5. The effective range along the anteroposterior direction of the gold markers in the upper lobes of the lung. Also indicated are the p values obtained from comparison of the effective ranges obtained in each patient setup.

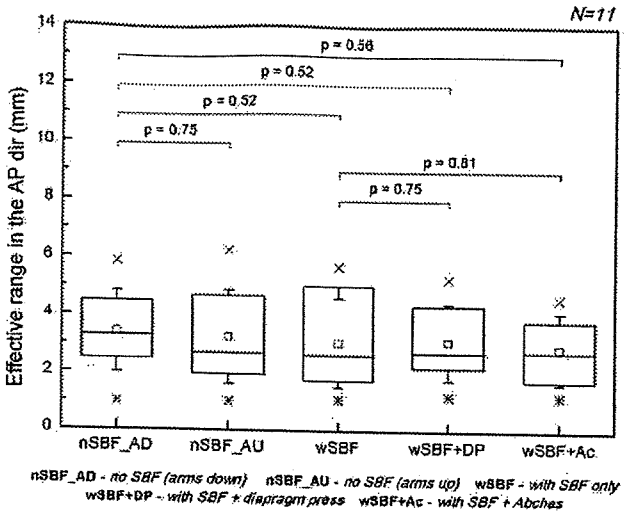

Fig. 6. The effective range along the lateral direction of the gold markers in the middle or lower lobes of the lung. Also indicated are the p values obtained from comparison of the effective ranges obtained in each patient setup.

3.39 mm in the AP direction (Fig. 5). The spread of the effective range values was largest along the CC direction, with a standard deviation of about 2.57–3.06 mm, and smallest along the LR direction, with a standard deviation of less than 1 mm. The maximum effective ranges of the markers obtained from the LR, CC, and AP directions were 3.73 mm, 10.13 mm, and 6.27 mm, respectively.

Motion of markers in the middle or lower lobes

As shown in Fig. 6, a slight variation in the mean effective range along the LR direction for the five setups was observed in the middle or lower lobe markers, with values between 2.18 mm and 2.98 mm; however, these differences were also not statistically significant (see The p values in Fig. 6).

The spread of the effective ranges for this group was greater than that for the upper lobe markers, which had standard deviations of 1.56–2.70 mm.

Shown in Fig. 7 are the effective ranges in the CC direction for the middle or lower lobe markers. Although the two setups without SBF had mean effective ranges greater than 10 mm and the mean effective ranges for the SBF setup and the SBF + diaphragm setup were less than 10 mm, the differences in the mean effective range between the setups were not statistically significant. The use of the Abches for this group of patients resulted in a mean effective range of about 13 mm. The standard deviations of the effective ranges in the CC direction were between 5.56 mm and 6.37 mm.

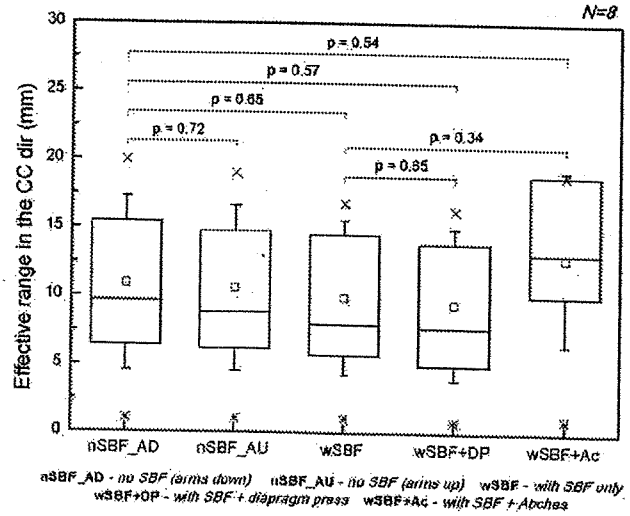

Fig. 7. The effective range along the craniocaudal direction of the gold markers in the middle or lower lobes of the lung. Also indicated are the p values obtained from comparison of the effective ranges obtained in each patient setup.

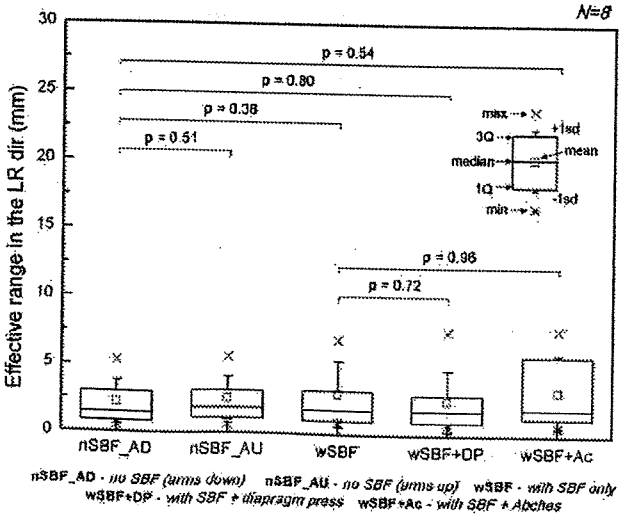

Fig. 8. The effective range along the anterior-posterior direction of the gold markers in the middle or lower lobes of the lung. Also indicated are the p values obtained from comparison of the effective ranges obtained in each patient setup.

The effective ranges in the AP direction for the middle or lower lobe markers were also greater than their upper lobe counterparts. The mean effective ranges shown in Fig. 8 for the five patient setups are between 3.61 mm and 5.04 mm with standard deviations between 2.45 mm and 4.81 mm. Again, no significant differences were noted among the five setups. The setup including the Abches had the largest mean effective range of 5.04 ± 4.81 mm.

DISCUSSION

In the present study, the real-time tracking capability of our RTRT system was used to determine the three-dimensional motion of fiducial gold markers embedded near or at the tumor to determine whether the respiration-induced motion of these markers can be controlled in free and restricted breathing setups. With the RTRT system, we were able to determine the instantaneous displacement of fiducial markers near the tumor, as has been done in previous studies (7, 15, 19, 20), as well as the full range of motion of these markers. This allowed a more comprehensive evaluation of the feasibility of controlling respiratory-induced motion by using an SBF, diaphragm press and breathing cycle monitor.

The motions of fiducial markers were found to be highly patient-dependent and were influenced by the location where the markers were embedded in the lung. In general, markers in the upper lobes exhibited a smaller range of motions along the LR, CC, and AP directions compared with the motions of the markers in the lower lobes, which are consistent with the previous results reported by Seppenwoolde *et al.* (3) and Onimaru *et al.* (16). The average effective ranges of marker motion in the present study were comparable with the amplitudes obtained in the three-dimensional analysis by Seppenwoolde *et al.* (3) of tumor motion in the lung in a setup without SBF and with the patient's arms down.

The markers in the upper lobe of the lung exhibited ranges of motions, which did not vary significantly irrespective of the patient setup used. Additionally, their maximum effective ranges, which were all observed in the CC direction, were <10 mm. Engelsmann *et al.* (21) have previously reported that respiration-induced tumor motion of up to 10 mm does not drastically change the dose distribution. Thus, the patient breathing control may no longer be necessary for the majority of tumors in the upper lobes of the lung.

The markers in the middle or lower lobes of the lung exhibited larger motion in the CC direction and larger spread in the individual effective ranges in the LR, CC, and AP directions. Thus, respiration-induced tumor motion management for tumors in the lower lobes is worth considering, if possible (21).

We evaluated five patient setups in this study with the goal of reducing respiration-induced tumor motion; however, we found that the effective range of marker motions in the lower lobes of the lung was not significantly different among these setups. This result is different from the pioneering studies of Lax *et al.* (7) and Negoro *et al.* (9), which attempted to limit the abdominal motion of patients using the SBF and a diaphragm press. However, the comparisons between setups with or without a diaphragm press in the two aforementioned studies were done with a smaller number of patients compared with the present study (7, 8). Lax *et al.* noted that the diaphragmatic motion was reduced from a range of 1.5–2.5 cm to a range of 0.5–1.0 cm in 17 patients evaluated using fluoroscopy (7). Negoro *et al.* found that tumor motion in the CC direction was reduced from 8–20 mm for the setup with SBF down to only 2–10 mm for the setup using SBF and diaphragm press in 10 patients (9). However, they also had 1 patient whose tumor movement of 7 mm increased to 10 mm upon the use of diaphragm control. Compared with the previous visual measurement using AP fluoroscopy, the present study measured the three-dimensional motion of the internal fiducial markers with more objective and reproducible methods. Thus the discrepancy in the results between these pioneering works and the present study may have been related to the methods used or the precision of the measurements, together with other factors such as the patient background (*e.g.*, tumor stage, location of tumors).

Additionally, although the tracking sessions were performed using a random sequence of patient setups, this may not have completely eliminated some bias due to patient setup, since by the time the patient goes through the last setup, he or she would have been on the couch for at least 20 min longer compared with the first setup. We also cannot neglect the possibility that some patients might have benefited from any of the setups evaluated in this study because of the relatively small patient population. However, it is not possible from our study to recommend the use of the SBF alone or in combination with the diaphragm press or the Abches as a universally effective method to control respiratory intrafractional organ motion.

In conclusion, our RTRT measurement of the effective range of motion of fiducial markers showed that using the SBF, the diaphragm press, or a breathing cycle monitor for the purpose of controlling the patient breathing does not generally result in smaller effective marker ranges. Whether these patient setups will be effective in reducing respiratory-induced organ motion should be examined for individual patients before using them in the radiotherapy.

REFERENCES

1. Keall PJ, Mageras GS, Balter JM, *et al.* The management of respiratory motion in radiation oncology report of AAPM Task Group 76. *Med Phys* 2006;33:3874–3900.
2. Shimizu S, Shirato H, Ogura S, *et al.* Detection of lung tumor movement in real-time tumor-tracking radiotherapy. *Int J Radiat Oncol Biol Phys* 2001;51:304–310.
3. Seppenwoolde Y, Shirato H, Kitamura K, *et al.* Precise and real-time measurement of 3D tumor motion in lung due to breathing

and heartbeat, measured during radiotherapy. *Int J Radiat Oncol Biol Phys* 2002;53:822–834.
4. Shirato H, Harada T, Harabayashi T, *et al.* Feasibility of insertion/implantation of 2.0 mm-diameter gold internal fiducial markers for precise setup and real-time tumor tracking in radiotherapy. *Int J Radiat Oncol Biol Phys* 2003;56: 240–247.
5. Shirato H, Shimizu S, Shimizu T, *et al.* Real-time tumour-tracking radiotherapy. *Lancet* 1999;353:1331–1332.
6. Shirato H, Shimizu S, Kunieda T, *et al.* Physical aspects of a real-time tumor-tracking system for gated radiotherapy. *Int J Radiat Oncol Biol Phys* 2000;48:1187–1195.
7. Lax I, Blomgren H, Naslund I, *et al.* Stereotactic radiotherapy of malignancies in the abdomen. *Acta Oncol* 1994;33:677–683.
8. Herfarth K, Debus J, Lohr F, *et al.* Extracranial stereotactic radiation therapy: Set-up accuracy of patients treated for liver metastases. *Int J Radiat Oncol Biol Phys* 2000;46: 329–335.
9. Negoro Y, Nagata Y, Aoki T, *et al.* The effectiveness of an immobilization device in conformal radiotherapy for lung tumor: Reduction of respiratory tumor movement and evaluation of the daily set-up accuracy. *Int J Radiat Oncol Biol Phys* 2001;50:889–898.
10. Ko Y, Suh Y, Ahn S, *et al.* Immobilization effect of air-injected blanket (AIB) for abdomen fixation. *Med Phys* 2005;32: 3363–1046.
11. Harada T, Shirato H, Ogura S, *et al.* Real-time tumor-tracking radiation therapy for lung carcinoma by the aid of insertion of a gold marker using bronchofiberscopy. *Cancer* 2002;95: 1720–1727.
12. Imura M, Yamazaki K, Shirato H, *et al.* Insertion of fiducial markers for setup and tracking of lung tumors in radiotherapy. *Int J Radiat Oncol Biol Phys* 2005;63:1442–1447.
13. Hof H, Herfarth K, Münter M, *et al.* Stereotactic single-dose radiotherapy of stage I non-small-cell lung cancer (NSCLC). *Int J Radiat Oncol Biol Phys* 2003;56:335–341.
14. Lohr F, Debus J, Frank C, *et al.* Non-invasive patient fixation for extracranial stereotactic radiotherapy. *Int J Radiat Oncol Biol Phys* 1999;45:521–527.
15. Nagata Y, Negoro Y, Aoki T, *et al.* Clinical outcomes of 3D conformal hypofractionated single high-dose radiotherapy for one of two lung tumors using a stereotactic body frame. *Int J Radiat Oncol Biol Phys* 2002;52:1041–1046.
16. Onimaru R, Shirato H, Fujino M, *et al.* The effect of tumor location and respiratory function on tumor movement estimated by real-time tracking radiotherapy (RTRT) system. *Int J Radiat Oncol Biol Phys* 2005;63:164–169.
17. Barnes E, Murray B, Robinson D, *et al.* Dosimetric evaluation of lung tumor immobilization using breath hold at deep inspiration. *Int J Radiat Oncol Biol Phys* 2001;50:1091–1098.
18. Shirato H, Oita M, Fujita K, *et al.* Feasibility of synchronization of real-time tumor-tracking radiotherapy and intensity-modulated radiotherapy from viewpoint of excessive dose from fluoroscopy. *Int J Radiat Oncol Biol Phys* 2004;60: 335–341.
19. Shirato H, Suzuki K, Sharp G, *et al.* Speed and amplitude of lung tumor motion precisely detected in four-dimensional setup and in real-time tumor-tracking radiotherapy. *Int J Radiat Oncol Biol Phys* 2006;64:1229–1236.
20. Mageras GS, Yorke E, Rosenzweig K, *et al.* Fluoroscopic evaluation of diaphragmatic motion reduction with a respiratory gated radiotherapy system. *J Appl Clin Med Phys* 2001;2: 191–200.
21. Engelsman M, Sharp G, Bortfeld T, Onimaru R, Shirato H. How much margin reduction is possible through gating or breath hold? *Phys Med Biol* 2005;50:477–490.

3D irradiation of pencil beam scanning for proton

Toru Asaba[1], Toshiki Tachikawa[1], Manabu Yamada[1], Toshiaki Ochi[1], Jun Inoue[1], Teiji Nishio[2], Takashi Ogino[2]

[1] Sumitomo Heavy Industries, Ltd, Quantum equipment division, Niihama, Ehime, Japan
[2] National Cancer Center Hospital East, Kashiwa, Chiba, Japan

Purpose

SHI has developed a new pencil beam scanning nozzle. Taking advantage of continuous and high intensity beam from cyclotron, the line scanning method is employed in order to realize continuous irradiation with high dose rate. 3D irradiation volume is divided into energy layers and each layer is irradiated with intensity modulated line scanning. The scanning nozzle was installed in the gantry of proton therapy system at NCCHE and the 3D irradiation test has been conducted.

Method

Modulation of dose distribution in each layer is done by varying the scanning speed and keeping the beam current constant. Intensity at different layer is adjusted by either changing the preset value of beam current or changing the number of rescanning. The beam intensity is made constant by stabilizing the extracted current from cyclotron with a feedback system. Energy scanning in each layer is done with a range shifter located at the nozzle exit.
3D dose distribution is measured by array of ionization chambers. Agreement with calculation is evaluated by gamma index criterion under 3mm/3% condition.

Result

Spherical target is chosen as one of the typical 3D irradiation field. Dose simulation is done by the original simulation software which will be presented in another session.

Conclusion

We developed the line scanning method and verified the agreement of calculation and measurement dose distributions for 3D spherical target by the gamma index.

Enhanced Radiobiological Effects at Distal-End of Proton SOBP Beam

Mami Wada[1], Yoshitaka Matsumoto[1], Taeko Matsuura[2], Yusuke Egashira[2], Sachiko Koike[1], Yuki Kase[1], Ayane Kanemoto[3], Teiji Nishio[2], Naruhiro Matsufuji[1], Yoshiya Furusawa[1]

[1] National Institute of Radiological Sciences, Research Center for Charged Particle Therapy, Chiba, Japan
[2] National Cancer Center Hospital East, Japan
[3] Tsukuba University, Japan

Purpose: Radiobiological efficiencies in distal-end part of proton SOBP beams may much higher than 1.1 that used as the RBE of SOBP beam in many proton therapy facilities. To confirm an actual biological efficiency in the position, we examine the efficiency with an *in vitro* cell system.

Material and Method: We used HSG cells that obtained from human salivary gland tumor, and have been used as a standard cell-line for RBE measurements at therapeutic ion beam facilities in Japan. The cells were maintained in Eagle-MEM medium supplemented with 10% FBS and antibiotics, and incubated under 5% CO_2 balanced with air at 37 dgrees C. Cell samples were prepared two days before irradiation at NIRS (Nat'l. Inst. Radiol. Sci.), home laboratory in Chiba, brought them to NCC/EH (Nat'l Cancer Cen., Hosp. East) in Kashiwa under a warm condition, and brought back in a cool condition just before and after the irradiation. Cells were irradiated with proton beam (190MeV, 5cm-SOBP, 100mm dia.) at different depths in the distal-end part and the center of the SOBP beam at NCC/HE. Central position of the SOBP was fixed at the iso-center of the beam, and depths of each sample were adjusted by placing polyethylene plates. All biological assays were performed at home laboratory. Surviving fractions were obtained, and killing efficiencies at each depth to the center were obtained. Biological dose distribution was calculated with the efficiencies and the physical doses at each position, and was compared with the physical dose distribution.

Results: Physical dose distribution was flat in the SOBP and decreased gradually at the distal-end of the SOBP. Biological efficiencies at the distal-end were higher than that at the center, and the efficiencies at all positions tested were approximately 1.2 to the center of the SOBP. This also means that the biological range of the beam is extended several millimeters to the down stream compared with physical dose distribution.

Conclusion: Biological dose at distal-end of SOBP beam was higher than that at the center of SOBP beam. This higher radiobiological efficiency extends the biological efficient range of the beam than that for physically defined dose distribution. This may causes side effects to healthy tissues at the distal position of the beam.

The biological effect of high-dose-rate proton beam on HSG cell

Taeko Matsuura[1], Yusuke Egashira[1], Teiji Nishio[1], Yoshitaka Matsumoto[2], Yoshiya Furusawa[2], Mami Wada[2], Sachiko Koike[2], Yuki Kase[2], Takashi Ogino[1]

[1] National Cancer Center Hospital East, Particle Therapy Division, Kashiwa, Chiba, Japan
[2] National Institute of Radiological Sciences, Research Center for Charged Particle Therapy, 4-9-1 Anagawa, Inage-ku, Chiba-shi, Chiba 263-8555, Japan

Purpose:
By taking the advantage of high intensity proton beam from AVF cyclotron and utilizing the projection images acquired during the treatment, we are developing a novel high-dose-rate proton therapy on tumors that move with respiration.
The dose rate is expected to be around ten or hundred times larger than the present dual-ring double scattering method. In order to investigate the biological effects of such a high-dose-rate proton beam, we performed clonogenic assay on HSG cell (JCRB1070:HSGc-C5). The survival curve as well as the relative biological effectiveness(RBE) are compared with those at normal dose-rate.

Methods:
HSG cells were attached to the bottom of the plastic flask(Lab-Tech SlideFlask, NUNC 170920) and irradiated by high (300nA, HDR) and low intensity (10nA, LDR) proton beams with the energy of 235MeV at NCCEH. The corresponding dose rate was 325Gy/min(8Gy/min) at Bragg-peak and 114Gy/min(1.75Gy/min) at plateau, respectively.
The spatial dose variation relative to the dose at beam central axis is within 2.5% over the cell attached area (2cmx5cm). The irradiation was performed both at Bragg-peak(high LET) and at plateau(low LET) in order to analyze the LET dependence. The irradiated dose ranged from 1Gy to 8Gy. EBT film was attached in front of the flask and the absorbed dose was measured simultaneously with the cell irradiation. The survival parameters were calculated from the data by fitting the survival curve by LQ model, $SF = \exp(-aD - bD^2)$, where SF stands for the survival fraction, and D is the dose exposed.
The $D_{10\%}$ values (dose which would reduce cell survival to be 10%) were obtained from the a and b parameters for each survival data set.

Results:
No significant splits were found among low and high dose-rate survival curves for both LET.
The RBE ratio between LDR and HDR, i.e. $RBE(LDR)/RBE(HDR)=D_{10\%}(HDR)/D_{10\%}(LDR)$, was 0.98 at Bragg-peak and 0.96 at plateau, which indicates the variation of RBE with the dose-rate can be ignored. On the other hand, the significant difference in RBE between high and low LET was found, RBE(high LET)/RBE(low LET)=1.13-1.20.
The good agreement of the result of EBT film and the irradiated dose prediction ensured the reliability of the experiment.

Conclusions:
We conclude that it is highly possible that the current RBE value is applicable for high-dose-rate proton therapy without modification. The LET dependence of RBE should be reconsidered for more accurate dose calculation.

In-vivo Dosimetry Using a MOSFET Detector in an Anthropomorphic Phantom for Therapeutic Proton Beam

Ryosuke Kohno[1], Kenji Hotta[2], Kana Matsubara[3], Taeko Matsuura[1], Satoru Kameoka[1], Teiji Nishio[1], Mistuhiko Kawashima[1], Takashi Ogino[1]

[1] National Cancer Center Hospital East, Particle Therapy Division, Chiba, Japan
[2] University of Tsukuba, Pure and Applied Sciences, Ibaraki, Japan
[3] Tokyo Metropolitan University, Graduate School of Human Health Sciences, Tokyo, Japan

Propose: For implementation of radiation therapy with proton beams in the clinics, comprehensive dose verifications are essential. In-vivo dosimetry can be used to identify major deviations in the delivery of treatment. Therefore, we think in-vivo dosimetry during patient treatment as the ultimate dose verification for patient quality assurance. In order to carry out in-vivo dosimetry, the detector must be very small, and easy to localize. To achieve this goal, we used metal oxide-silicon field-effect transistor (MOSFET) detectors. Here, the MOSFET response depends strongly on the degree of linear energy transfer (LET) of the proton beam. Therefore, for correcting the MOSFET response to proton beams, we developed a new method, which calculates the correction factor of the MOSFET detector using the simplified Monte Carlo dose calculation method (SMC).
Methods: The depth-output curve in polyethylene for mono-energetic proton beam was measured by using the MOSFET detector. The SMC (SMC^{MOSFET}) uses this depth-output curve to calculate MOSFET output distributions. Then, the MOSFET output values at an arbitrary point obtained by this SMC^{MOSFET} were compared with the dose obtained by the conventional SMC, which uses the depth-dose curve was measured by using the ionization chamber. From the ratio of both values, we can calculate the correction factor of the MOSFET detector at the arbitrary point. Finally, the dose measured by the MOSFET detector at the arbitrary point is given by the product of the correction factor and the MOSFET raw dose without correcting. We performed in-vivo proton dosimetry by using the MOSFET detector with the RANDO phantom as an anthropomorphic phantom for the first time. Dose measurements were carried out in the head and neck region. MOSFET doses with correction were compared with the calculations obtained by the SMC and the dose measured by the MOSFET without correction.
Results: The results measured by the MOSFET without correction indicates a remarkable deviation from the result of the SMC. This means that the MOSFET responses changed. On the other hand, the MOSFET doses with correction agreed with the SMC results within the measurement error.
Conclusions: In order to measure dose distributions using a MOSFET detector, we developed a new method for correcting the MOSFET response to proton beams. For doses in the RANDO phantom, the MOSFET dose agreed well with the SMC results within the measurement error. In-vivo proton dosimetry could be successfully performed using MOSFET detectors for the first time.

Fine-pitch multi-leaf collimator for proton therapy system

Toshiki Tachikawa[1], Yutaka Arai[1], Toshiaki Ochi[1], Teiji Nishio[2], Takashi Ogino[2]

[1] Sumitomo Heavy Industries, Ltd., Quantum Equipment Division, Niihama, Japan
[2] National Cancer Center Hospital East, Particle Therapy Division, Kashiwa, Japan

Fine-pitch multi-leaf collimator for proton therapy system

Toshiki Tachikawa[1], Yutaka Arai[1], Toshiaki Ochi[1],
Teiji Nishio[2] and Takashi Ogino[2]
[1]Sumitomo Heavy Industries, Ltd. (SHI)
[2]National Cancer Center Hospital East (NCCHE)

Purpose : Multi-leaf collimator (MLC) in special use for proton therapy system has been developed and its performance has been tested. Although the new MLC has fine pitch leaves and wide collimator opening, its size is kept compact so that it can be installed in the gantry nozzle and can be rotated around the irradiation axis.

Methods : The new MLC has leaves of 3mm and 5mm thickness, and the maximum mechanical opening is 185mm x 185mm. Irradiation field size at isocenter is 200mm x 200mm when the MLC is located at minimum distance (270mm) from isocenter. Each leaf is driven by a pulse motor and its position is monitored by a potentiometer. All mechanical components are placed inside a circle of 900 mm diameter and can be rotated +/- 90 degree around the irradiation axis.

Results : Driving durability test of prototype was performed at SHI factory, and normal operation without any mechanical failure was proven after 200,000 cycles of reciprocation. The MLC has been installed in a gantry for wobbling system, and performance test using 230MeV proton beam will be started in March 2010.

Conclusions : Fine pitch and compact multi-leaf collimator has been developed and its mechanical performance has been evaluated. Results of irradiation tests will be presented.

Development of Beam Position Monitoring System for Pencil Beam Scanning

Junichi Inoue[1], Masanori Tachibana[1], Toshiaki Ochi[1], Takuzo Morita[1], Toshiki Tachikawa[1], Toru Asaba[1], Masayuki Hirabayashi[1], Yukio Kumata[1], Teiji Nishio[2], Takashi Ogino[2]

[1] Sumitomo Heavy Industries, Ltd., Quantum Equipment Division, Ehime, Japan
[2] National Cancer Center Hospital East, Kashiwa, Chiba, Japan

Purpose: SHI has been developing a new beam position monitoring system for pencil beam scanning irradiation in collaboration with NCCHE. It is important to detect precise irradiation beam spot position in short interval time to prevent normal tissues from being irradiated. The purpose of this article is to summarize the design and evaluations of beam position monitoring system that improves quality of treatment.

Methods: The beam position monitoring system consists of two main parts, one is sensing equipment which has two directional grid wires(X-Y grid wires) and electrical amplifiers to convert electricity from proton beam into voltage signal. The other is digital processing unit which has high speed calculator to recognize scanning beam spot position. The sampling time of beam sensing is less than 0.2msec and this value is equivalent to 2mm in case of maximum scanning speed of 10mm/msec. The digital processing unit also calculates the gravity center of beam spot. The spatial resolution of gravity center is less than 1 millimeter. After calculation of beam position, the processor compares actual position with planned position of scanning beam. If scanning beam spot missed the planned beam path, the processor would cause interlock event immediately.

Results: A test model of the sensing equipment and the electrical amplifiers which has two channels was assembled and tested at NCCHE by using actual proton beam and the results showed that the signal was enough good to detect scanning beam spot.

Conclusions: Development of a new beam monitoring system has been conducted and a test model was evaluated at NCCHE. By installing this new monitor system and combination with other beam monitor systems, precise and safe irradiation of pencil beam scanning is achieved.

Improvement of beam-use efficiency for double-scattering method using a multiple-ring second scatterer in proton therapy

Yoshihisa Takada[1], Kenji Hotta[1], Ryohsuke Kohno[2], Takeshi Himukai[3], Yousuke Hara[1], Teiji Nishio[2]

[1] University of Tsukuba, Institute of Applied Physics, Tsukuba, Ibaraki, Japan
[2] National Cancer Center Hospital East, Kashiwa, Japan
[3] National Institute of Radiological Sciences, Chiba, Japan

Background

We developed a conceptual design of a noble double scattering method using a second scatterer with multiple-concentric-ring structure made from bi-materials. Theoretical limit of the attainable beam-use efficiency was found to be about 60% for a beam with low-emittance. We verified the scheme by measurements and obtained a beam-use efficiency of 50% that is more than the maximum of current techniques even under a limited experimental condition.

Materials and Method

We manufactured a second scatterer with octuple concentric-ring structure intending to use it for 200-MeV beam in a certain beam-line arrangement. Each ring element is comprised of a chemical wood and a Pb-Sb alloy. The scattering strength was tuned by changing the combination.

We measured the dose distribution using a 178-MeV proton beam of National Cancer Center Hospital East and a small parallel-plate ionization chamber with 5 mm lateral spatial resolution scanned in water. We placed an additional ring collimator with an aperture diameter of 5 or 10 mm as an option in front of the first scatterer to reduce the initial beam size. Since we applied the multiple-ring scheme to the existing beam line, we had some experimental restrictions. Then we performed the experiment under a limited condition resulting in the expected beam-use efficiency of about 50% lower than the theoretical maximum. We set the 1/e scattering radius of the first scatterer at 68.0 mm and expect the usable region of a circular region with a radius of about 76 mm.

Results and Discussion

We attained beam-use efficiency of 50% for an initial beam defined by the ring collimator with an aperture diameter of 5 mm. The value is consistent with calculation. When we removed the additional ring collimator, beam-use efficiency reduced to 44%. We also found that reduction of beam-use efficiency by addition of a range shifter can be partly restored by longitudinal position control of the second scatterer.

Difference between this method and the existing one using a bi-material contoured scatterer is that the former increases contribution of protons scattered in the outer part of the rings into the usable inner region.

Conclusion

We have verified efficacy of the new scheme of double scattering using a bi-material second scatterer with multiple concentric-ring structure. We achieved beam-use efficiency of 50% under a limited experimental condition. There remains a possibility to increase the efficiency up to about 58% if we would design a fully optimized second scatterer.

The clinical use of the beam ON-LINE PET system mounted on a rotating gantry port in proton therapy

Teiji Nishio[1], Aya Miyatake[1], Toshiki Tachikawa[2], Manabu Yamada[2], Takashi Ogino[1]

[1] Research Center for Innovative Oncology National Cancer Center Hospital East, Kashiwa, Particle Therapy Division, Chiba, Japan
[2] Sumitomo Heavy Industries, Ltd., Quantum Equipment Division, Ehime, Japan

Proton therapy is a form of radiotherapy that enables the concentration of a dose onto a tumor by the use of a scanned or modulated Bragg peak. Therefore, it is very important to evaluate the proton-irradiated volume accurately. The proton-irradiated volume can be confirmed by detection of pair-annihilation gamma rays from positron-emitting nuclei generated by the target nuclear fragment reactions of the incident protons on target nuclei using a Positron Emission Tomography (PET) apparatus, and so dose-volume delivery guided proton therapy (DGPT) can thereby be achieved using PET images.

A beam ON-LINE PET system mounted on a rotating gantry port (BOLPs-RGp) was constructed in our proton treatment room. Detector heads of the planar type with a high spatial resolution of about 2 mm were mounted with the field of view covering the iso-center of the rotating gantry system. The activity observed at each proton irradiation angle, measured with the BOLPs-RGp, was immediately captured using real-time imaging during daily proton treatment. The images obtained were compared with the proton dose distributions calculated by a proton treatment planning system. Moreover, the images obtained from the proton irradiation can be stored, and changes in the activity distribution and/or the intensity can be viewed in series and later analyzed. As a result, a high quality proton therapy can be provided to patients. The BOLPs-RGp was used daily in cases involving tumors of the brain, head and neck, liver, lungs, and prostate. It was confirmed that the BOLPs-RGp was useful for providing quality assurance, quality control, and a high accuracy of proton therapy.

Initial Evaluation of Delta-functional Multi Segmented Pencil Beam Algorithm for Proton Therapy

Yusuke Egashira[1], Teiji Nishio[2,3], Satoru Kameoka[3], Taeko Matsuura[2,3], Mitsuru Uesaka[1]

[1] University of Tokyo, Department of Bioengineering, Graduate School of Engineering, Tokyo, Japan
[2] University of Tokyo, Radiology and Biomedical Enginnering, Graduate School of Medicine, Tokyo, Japan
[3] National Cancer Center Hospital East, Research Center for Innovative Oncology, Kashiwa, Japan

[Purpose] Dose calculation methods by the pencil beam algorithm (PBA) are currently most commonly used for proton therapy treatment planning. It utilizes the one-dimensional density scaling along the central axis of the pencil beam and the off-axis density heterogeneity is neglected, i.e. the lateral dose spread by proton multiple Coulomb scattering is calculated only along the central axis. Therefore it can lead a considerable error in the dose distribution if the beam passes the complicated structures in a patient body. In order to take into account the effect of heterogeneity materials in a patient body, we propose a novel and more accurate dose calculation algorithm, delta-functional multi segmented pencil beam algorithm (DMS-PBA). In this study, the initial verification of DMS-PBA was carried out as a first step towards the clinical use of proton therapy.
[Methods] DMS-PBA method is based on surface-map analysis and beam segmentation on the surface of patient body. Surface-map analysis determines the number of segmented daughter pencil beams: beamlets on the each surface calculation grid. The initial beam emittance of each segmented beamlets is very small, corresponding to the delta-function. The total dose distribution is obtained by integration over all beamlets. For the dose verification, we used the L-shaped polyethylene block, which represented the lateral heterogeneity of a medium. It was set above the polyethylene plates and the three dimensional dose distributions were measured with the two-dimensional detector put under the polyethylene plates. The simulation was done using DMS-PBA as well as conventional PBA for comparison.
[Results] In measurement, hot/cold spots were detected at z = 123, 142, 162 mmWEL. Conventional PBA method could reproduce none of these singular points and the dose difference amounted to about 12 %. On the other hand, DMS-PBA and measurements generally agreed well, considering that the experimental errors in device alignment could have been 1 mm or more. The hot/cold spots measured in the dose distributions may reflect the difference of proton trajectories at the border between polyethylene and air. DMS-PBA could reproduce the proton detour and overreaching effect by utilizing the delta-functional initial beam emittance of each beamlet.
[Conclusions] We showed that our proposed method, DMS-PBA, could improve the accuracy of dose calculation for treatment planning of proton therapy.

PTCOG 48

September 28th - October 3rd, 2009
Heidelberg Convention Center

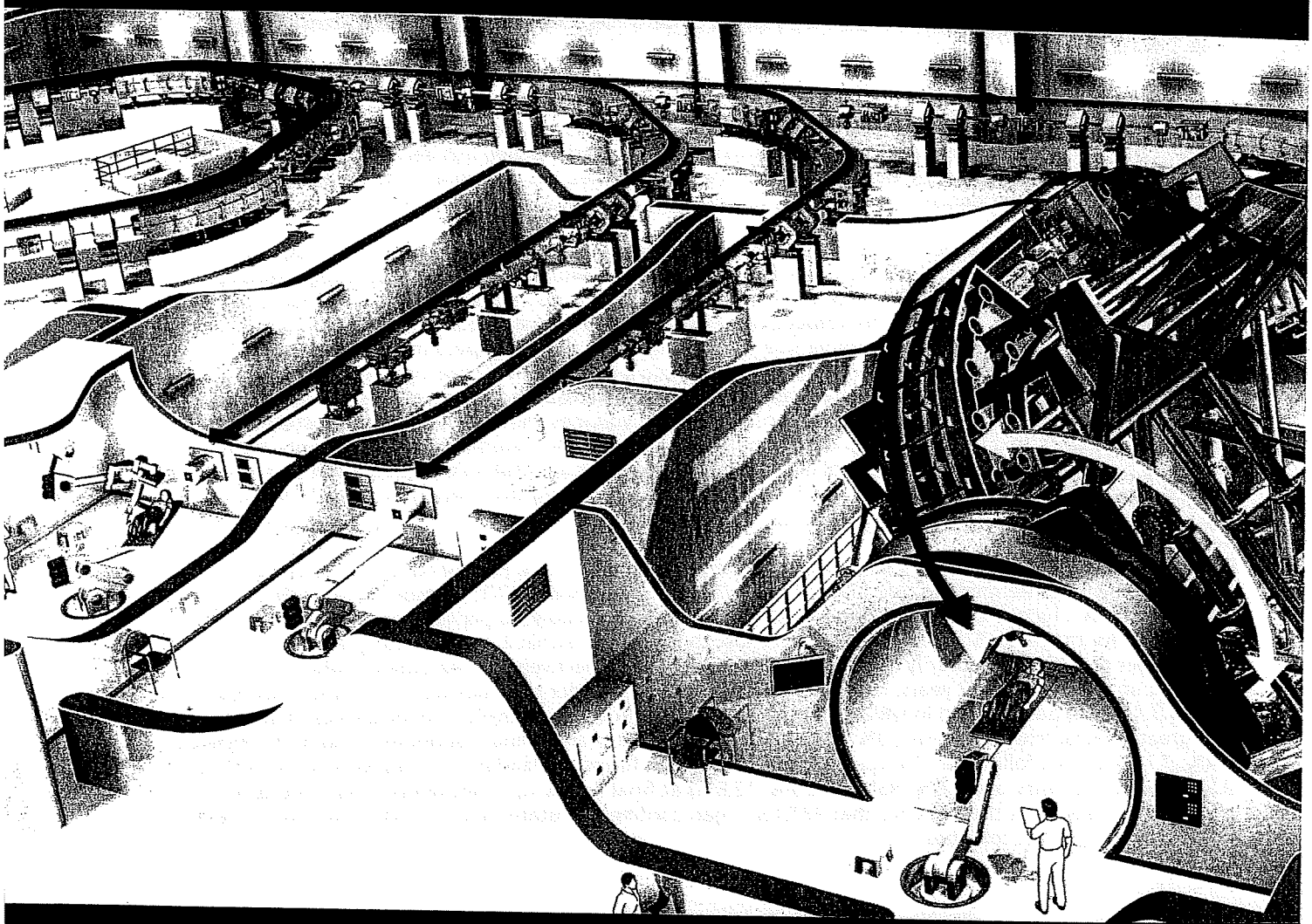

Abstract book

Congress-President

Jürgen Debus, MD PhD

UniversitätsKlinikum

NCT NATIONALES CENTRUM FÜR TUMORERKRANKUNGEN HEIDELBERG

dkfz DEUTSCHES KREBSFORSCHUNGSZENTRUM

HIT Heidelberger Ionenstrahl-Therapiezentrum

GSI Forschungszentrum

Particle Therapy Co-Operative

Conclusion:
It is feasible to treat prostate cancer with protons in the presence of unilateral hip replacement by modifying the treatment approach, substituting the lateral field from the side of the replaced hip with 2 anterior oblique fields.

FC63

Multi-Institutional Phase II Study of Proton Beam Therapy for Organ Confined Prostate Cancer in Japan, Focusing on the Incidence of Late Rectal Toxicities.

K. Nihei[1], M. Onozawa[1], T. Ogino1, S. Murayama[2], H. Fuji[2], M. Murakami[3], Y. Hishikawa[3]
[1]National Cancer Center Hospital East, Kashiwa, Japan; [2]Shizuoka Cancer Center, Shizuoka, Japan; [3]Hyogo Ion Beam Medical Center, Tatsuno, Japan;

Background:
Proton beam therapy (PBT) for prostate cancer can provide a good dose distribution using simple bilateral opposed fields without increasing excessive doses to the rectum and bladder. But because the prospective data is lacking, it's not clear if PBT can clinically reduce the toxicities. We started a multi-institutional phase II trial focusing on the incidence of late grade 2 or greater rectal toxicity.
Material and Methods:
The major eligibility criteria included, 1) clinical stage T1-2N0M0, 2) initial PSA of 20 ng/ml or less, and Gleason score (GS) of 7 or less, 3) no hormonal therapy (HT) or HT within 12 months before registration, and 4) written informed consent. The low and intermediate risk groups in this study were defined as GS < 7 and PSA < 10, and GS = 7 or PSA > 10, respectively. Primary endpoint was the incidence of late grade 2 or greater rectal toxicity at 2 years. The sample size was set of 150, so that its upper limit of 95% confidence interval (CI) should be below 16% when the actual incidence is below 10%. Three institutions providing PBT in Japan participated in this study after each institutional review board approved this study. PBT was delivered to a total dose of 74 GyE in 37 fractions. The target volumes were defined as the prostate alone for low risk patients, and the prostate and proximal seminal vesicles for intermediate risk patients. Patients were prospectively followed up to collect the data of toxicities and PSA values one month and every 3 months after the completion of PBT for the first 2 years, and every 6 months thereafter. NCI-CTC version 2.0 was used to assess both acute and late toxicities.
Results:
From March 2004 to March 2007, 151 patients were enrolled in this study. Patients characteristics were as follows: low risk/intermediate risk, 77/74; T1c/T2a/T2b/T2c/T3a, 75/49/9/17/1; Gleason score 4/5/6/7, 5/15/80/51; iPSA <10/10-20, 102/49; HT/no HT, 42/109. The median follow-up period among all patients is 43.4 months (range: 3 - 62). Four patients were lost to follow-up within 2 years. Acute grade 2 rectal and bladder toxicities temporarily occurred in 0.7% and 12%, respectively. Of 147 patients who had been followed up for more than 2 years, late grade 1/2/3 rectal and bladder toxicities were observed in 27/5/0 (18.4%/3.4%/0%) patients and in 9/8/2 (6.1%/5.4%/1.4%) patients, respectively. The incidences of late grade 2 or greater rectal toxicities were 2.0% (95% CI; 0%, 4.3%) at 2 years (primary endpoint), and 4.1% (95% CI; 0.4%, 7.7%) at final follow-up. The corresponding figures in terms of bladder toxicities were 4.1% (95% CI; 0.9%, 7.3%) at 2 years, and 7.8% (95% CI; 2.9%, 12.8%) at final follow-up. Conclusion: These results of this prospective study show the evidence that PBT for organ confined prostate cancer can achieve low incidence of both acute and late toxicities.

FC66

Relative biological effectiveness of carbon ions in normal tissue and tumors

Chr. P. Karger[1], P. Peschke[2], M. Scholz[3], P. E. Huber[2], J. Debus[4]
[1]Medical Physics in Radiation Oncology, German Cancer Research Center (DKFZ), Heidelberg; [2]Clinical Cooperation Unit Radiation Oncology, German Cancer Research Center (DKFZ), Heidelberg; [3]Dept. of Biophysics, Gesellschaft für Schwerionenforschung (GSI), Darmstadt; [4]Dept. of clinical Radiology, University Clinic Heidelberg, Heidelberg;

Background: To determine the relative biological effectiveness (RBE) of carbon ions in the spinal cord and in a prostate tumor of the rat.
Material and Methods: The cranial part of the spinal cord of rats was irradiated with 1, 2, 6 or 18 fractions (Fx) of photons or carbon ions (in the plateau or in the middle of a 1 cm spread-out Bragg peak, SOBP), respectively. Biological endpoint was the onset of paresis grade II. In addition, a prostate carcinoma (R3327-AT1) implanted at the hind limb of the rats was irradiated with 1 or 2 Fx of photons or a 2 cm SOBP of carbon ions, respectively. An experiment with 6 Fx is ongoing. Endpoint of these experiments was local tumor control after one year. For all experiments, dose response curves and RBEs were calculated.

The beam ON-LINE PET system mounted on a rotating gantry port for proton therapy in National Cancer Center, Kashiwa

Nishio T[1,2], Miyatake A[3], Tachikawa T[4], Yamada M[4]

[1]Particle Therapy Division, Research Center for Innovative Oncology National Cancer Center Hospital East, Kashiwa, Japan

[2]Department of Radiology, Graduate School of Medicine, University of Tokyo, Tokyo, Japan

[3]Department of Nuclear Engineering and Management, Graduate School of Engineering, University of Tokyo, Tokyo, Japan

[4]Quantum Equipment Division, Sumitomo Heavy Industries, Ltd., Japan

Background: Proton therapy is one form of radiotherapy in which the irradiation can be concentrated on a tumor using a scanned or modulated Bragg peak. Therefore, it is very important to evaluate the proton-irradiated volume accurately. The proton-irradiated volume can be confirmed by the detection of pair annihilation gamma rays from a positron emitter nuclei generated by the nuclear fragmentation reaction between the incident proton and nuclei in the human body. This is accomplished by using a beam ON-LINE PET system (BOLPs) which uses PET images to carry out dose-volume delivery guided proton therapy (DGPT). The purpose of our study is to verify the utility of this developed system in clinical use.

Material and Method: In the proton treatment room, the BOLPs mounted on the rotating gantry port (BOLPs-RGp) were constructed so that a planar PET apparatus with spatial resolution as high as 1.6-2.1 mm could be mounted with the field of view covering iso-center of the beam irradiation system. The useful field size for the detection area is 164.8×167.0 mm^2. The BOLPs-RGp is set up with a 300-900 mm distance between the upper and lower opposing detector heads. The detector heads rotate around the iso-center synchronous with the rotating gantry port. Activity measurements were performed in 100 patients with tumors of head and neck, liver, lungs, prostate, and brain. The position and intensity of activity were measured using the BOLPs-RGp immediately after the proton irradiation. The measurement time was carried out between a period of 210–500 seconds (beam off: 200 seconds = constant) from the start of the proton irradiation. The measured data were stored in a computer for image display and for the analysis of the binary formatted data pixels with 1.1-mm size mapped on a frame of 164.8×167.0 mm^2 every second.

Results: The daily measured activity-images acquired by the BOLPs-RGp showed the proton irradiation volume in each patient. Changes in the proton-irradiated volume were indicated by differences between a reference activity-image (taken at the first treatment) and the daily